Title	Orbit Segmentation by Surface Reconstruction with Vertex screening
Author(s)	Hsung, TC; Lo, J; Chong, MM; Cheung, LK; Goto, T
Citation	The 19th International Conference on Digital Signal Processing (DSP), Hong Kong, China, 20-23 August 2014. In the Proceedings of the International Conference on Digital Signal Processing, 2014, p. 521-524
Issued Date	2014
URL	http://hdl.handle.net/10722/198603
Rights	Proceedings of the International Conference on Digital Signal Processing. Copyright © I E E E.

Orbit Segmentation by Surface Reconstruction with Vertex screening

Tai-Chiu Hsung, John Lo, Mei-Man Chong and Lim-Kwong Cheung
Discipline of Oral and Maxillofacial Surgery,
Faculty of Dentistry, The University of Hong Kong
Hong Kong
e-mail: tchsung@hku.hk

Tazuko K. Goto
Discipline of Oral Diagnosis and Polyclinics,
Faculty of Dentistry, The University of Hong Kong
Hong Kong

Abstract—**We suggest a computational approach to the orbit segmentation for computer tomography (CT) images. The first step was to perform Hounsfield unit thresholding to segment the bony structure. Then a three dimensional (3D) mesh model was generated. Poisson surface reconstruction was applied to the screened vertices that lay on the inner orbital walls. These procedures effectively interpolate the broken surfaces due to orbital fissures; various nerves foramina; and thin bone structure around the orbit. A validation was performed on the CT images of a dried skull with dental impression material filled orbits. The volume differences are 2.2 and 1.5% respectively for the two orbits. Surface differences are within ±0.46mm RMS. The differences are not clinically significant. The main novelty of proposed method is the ability in selecting vertices according to the desired orientation and therefore it is robust against broken structure in the segmentation.**

Keywords—Orbit, Biomedical imaging, Image segmentation, Computed Tomography, Surface fitting

I. INTRODUCTION

In eye anthropometry [1]-[3], the shape of the orbit (the cavity containing eyeball and its appendages) is very important. It provides necessary information for craniofacial surgery planning and assessment that involving the eyes [4]-[10]. The bony structure information founds application in the design of eye protection equipment. The statistical study gives correlation to the discovery of dimensional difference in sex, ethnic and age etc. However, segmentation of the orbit is challenging. Orbital walls and floor adjacent to para-nasal sinuses and the spongy ethmoid bones usually result in broken surfaces due to the partial volume effects. The gaps, fissures and various nerves foramina further complicate the measurement of the effective volume of orbit.

Currently, orbit segmentation are performed by, 1) Slice by slice segmentation; 2) Hybrid approach: live-wire and shape based interpolation [9]; 3) User guided 3D active contour segmentation (ITK-Snap) [14]; and 4) Interactive segmentation with haptic device [12].

In the slice by slice segmentation, each slice is segmented manually. It is usually aided with local Hounsfield unit thresholding with appropriate soft tissue and/or hard tissue windows. Although there are many tools that may aid the 2D segmentation [6]-[8] (for closed objects), it is still a labor demanding approach and usually requires 15 to 30mins to complete only one orbit segmentation. Furthermore, it exhibits inter- and intra- operator variability.

More advanced approach is to automatically interpolate the slices after segmented some slices manually. For example in the hybrid approach [9], interactive live-wire segmentation is applied to several slices in the interested volume. Then the shape-based interpolation is applied to generate the whole 3D models. It is further refined by using radial basis function to wrap the models with some specified fixed points. Another similar technique is suggested [10] in using OsiriX Medical imaging software. The approach is to draw ROI for several slices and group them for the orbit volume measurement.

3D active contour approach (ITK-snap) [14] could also be used to the orbit segmentation. By using edge image as preprocessing image with appropriate value in the scale and smoothing, accurate 3D model can be obtained. However, it often happens that many leakages appear from the nasolacrimal duct, superior and inferior orbital fissures etc. Further manual operations for subtracting out the leakages are usually necessary. Another approach is to make use of expert knowledge to guide the 3D shape interpolation using haptic device [12]. The user can define some fixed points, and edit the reconstructed model interactively. The orbit models are generated automatically.

Current methods are able to produce nice segmentation results but manual editing is still necessary. In this paper, we consider to construct the orbit model from the orbital bone model without interactive painting. It performs the processing on vertices rather than on voxels. We also validate the proposed method with a dried skull (Fig. 1).

II. METHODS AND MATERIALS

Firstly, a CT scan covering the interested orbit is obtained. We adopted the 3D Slicer platform [15] for the CT images

analysis, segmentation and visualization. Under this platform, the segmentation results are represented as voxel label volume. We can mark the label voxel from Hounsfield unit thresholding. 3D editing and filtering can also be applied on the label volumes. 3D mesh models can be generated from the label volumes. 3D models can also be sampled to generate a label volume. For the vertex screening, we perform the simulation in the Matlab (version R2012b, Mathworks, USA) platform. 3D Mesh model data are interchanged in using the Wavefront OBJ format. The proposed orbit segmentation method consists of a series of steps,

1. Orbital bone segmentation using Hounsfield unit thresholding (bone and air windows).
2. Vertex screening on inner orbital bone surfaces.
3. Poisson surface reconstruction with the selected vertices.
4. Cut model at anterior orbit boundary.

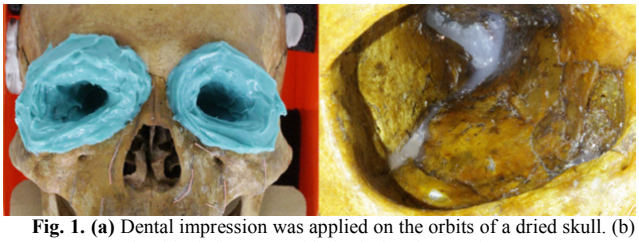

Fig. 1. (a) Dental impression was applied on the orbits of a dried skull. (b) wax are used to block fissures and holes before impression.

A. Orbital bone segmentation

Hounsfield unit thresholding is used for the segmentation of orbital bone. Interested region is cut for the construction of 3D models, as shown in Fig. 2. In this figure, a dried skull filled with dental impression on the orbital walls is studied. Thesholding with 400Hu is firstly applied to segment the bone. The medial wall and orbital floor are further segmented with a Hounsfield window -300 to 200Hu in the axial view. Alternatively, these boundaries could also be defined by segmented air in the sinuses. After these steps, voxel based morphological dilation (with four neighbors) is applied on the label volume. This prevents the final orbit model from overlapping with the orbital bone model.

B. Vertex screening for orbit inner surface reconstruction

Traditionally, the orbit shape is obtained by taking dental impression on the orbital walls with fissures and holes closed with wax. This effectively performed interpolation. To imitate this, we aim to obtain a closed orbit 3D model from the segmented orbital bone model. The resulted 3D model should respect the bone boundaries geometry and close all broken surfaces. Therefore, we suggest selecting vertices from the orbital bone model for the surface reconstruction [13] of orbit. The selected vertices should correspond to the definition of orbit cavity without holes, excessive leakages.

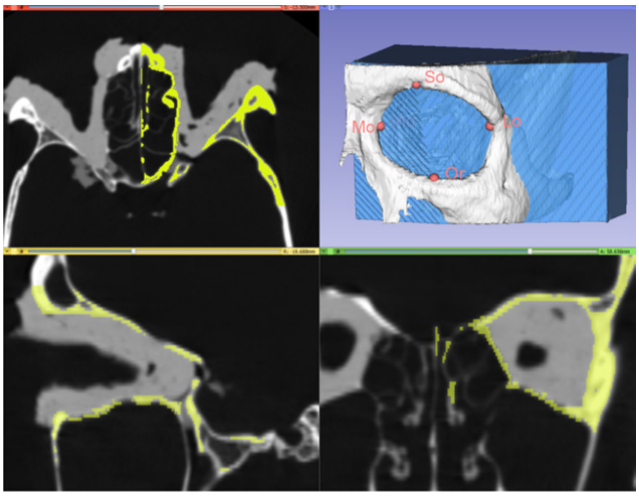

Fig. 2. Orbital bone is segmented using Hounsfield value thresholding (400Hu) for a dried skull. The orbits are filled with dental impression material (200-350Hu). Top right is 3D view showing the segmented orbital bone and anterior orbital boundary defined by two planes passing through So-Or-Mo and So-Or-Lo respectively.

Let us introduce the vertex screening primitives as: 1) The vertex defines the orbit inner surfaces; 2) The vertex does not contribute to the definition of holes, and their openings. In other words, we should only select the vertices that can be seen from a point inside the orbit. Let us denote the vertex set $\boldsymbol{B} = \{\boldsymbol{v}_r^b = (\boldsymbol{p}_r^b, \boldsymbol{n}_r^b): r = 1, \dots N_b\}$ to be the vertices of segmented orbital bone model; and the parameter model vertex set $\boldsymbol{S} = \{\boldsymbol{v}_k^s = (\boldsymbol{p}_k^s, \boldsymbol{n}_k^s): k = 1, \dots N_s\}$ where $\boldsymbol{p}, \boldsymbol{n} \in \mathbb{R}^3$ indicate the 3D coordinate and normal vector of a vertex in Cartesian coordinate respectively. We further denote the vector joining $\boldsymbol{v}^s$ and $\boldsymbol{v}^b$ as,

$$\boldsymbol{n}^{sb} = \boldsymbol{p}^s - \boldsymbol{p}^b \tag{1}$$

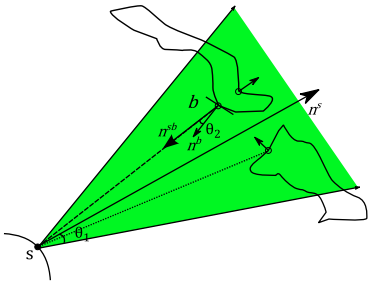

Fig. 3. Vertex screening: For a parameter vertex *s*, its field of view (green) is a cone with angle θ_1 along the direction of its normal $\boldsymbol{n}^s$. Vertices from orbital model fall into the field are considered. Only the vertices facing to s (with a tolerance θ_2) are included. The selected vertices patches are further screened according to the distance to *s*.

As shown in Fig. 3, given vertex $\boldsymbol{v}_k^s \in \boldsymbol{S}$, consider including vertices $\boldsymbol{v}_r^b \in \boldsymbol{B}$ if they fall into the field of view (in

green). That is, it is included if the angle θ between $\boldsymbol{n}^{sb}$ and $\boldsymbol{n}^{s}$ is less than a threshold, i.e. $\theta < \theta_1$ where

$$\cos\theta = (\boldsymbol{n}_r^{sb} \cdot \boldsymbol{n}_k^{s})/(|\boldsymbol{n}_r^{sb}||\boldsymbol{n}_k^{s}|) \quad (2)$$

Here θ_1 is used as a threshold to define the span of view. Here we omitted the indices in θ for clarity. The vertices from $\boldsymbol{B}$ fall into this field are considered. They are selected if facing to $\boldsymbol{v}_k^s$ within a tolerance θ_2, i.e.,

1. $\boldsymbol{v}_k^s$ is on the +ve side (facing to $\boldsymbol{v}_k^s$) of tangent plane of $\boldsymbol{v}_r^b$ relative to $\boldsymbol{p}_r^b$,

$$(\boldsymbol{p}_k^s - \boldsymbol{p}_r^b) \cdot \boldsymbol{n}_r^b > 0 \quad (3)$$

2. And projection angle of $\boldsymbol{n}_r^b$ to $\boldsymbol{n}_r^{sb}$, $\theta < \theta_2$ where

$$\cos\theta = (\boldsymbol{n}_r^{sb} \cdot \boldsymbol{n}_r^{b})/(|\boldsymbol{n}_r^{sb}||\boldsymbol{n}_r^{b}|) \quad (4)$$

In this way, vertices of the surfaces that are facing to the parameter vertex are selected. In order to eliminate the selection of orbital bone structures those are also facing to the parameter vertex but not the closest, we apply a simple clustering according to distance. Only the cluster (3mm diameter) at the closest distance to the parameter vertex is selected.

In the simulation, two spheres are created as parameter model for the vertex screening of orbital bone inner surfaces. They are located at the anterior and apex region of the orbit. Fig. 4(a) shows the orbital bone and parameter model (in red). There are 1280 and 480 vertices respectively for the anterior and apex sphere. In Fig. 4(b), it shows the selected vertex points (red) using the proposed vertex screening method. In this figure, the results are obtained with θ_1 and θ_2 set to 5 degrees.

Selected vertices are then used for the Possion surface reconstruction [13][16]. The anterior opening of the orbit is closed by simply mirror the selected vertices at the front. This result a closed reconstructed model and it can further be cut at the anterior orbit boundary.

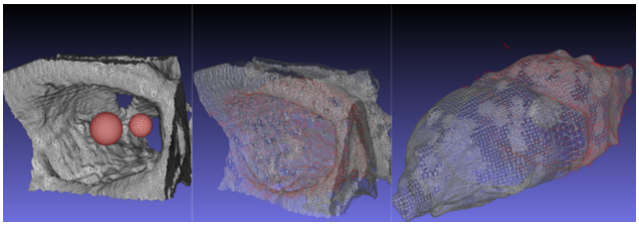

(a) **(b)** **(c)**

Fig. 4. Two spheres are created as parameter model for the vertex screening of orbital bone inner surfaces: (a) Orbital bone and parameter spheres (in red). (b) Selected vertex points (red). (c) Poisson surface reconstruction from the selected vertex points.

C. *Anterior orbit boundary*

In order to enable accurate volume comparison, we define two vertical planes at the orbital rim to serve as anterior boundary. The planes pass through three of the four landmarks respectively So-Or-Mo and So-Or-Lo; where the landmarks are: Supraorbitale (So), Orbitale (Or), Medio-orbitale (Mo), latero-orbitale (Lo). They are illustrated in Fig. 2. The model cutting is achieved by masking the segmented orbit model with a label volume that, each label are tested and set to one if they lie posterior to the planes defined by So-Or-Mo and So-Or-Lo. We implemented this label volume computation as a 3D Slicer 4 (with Matlab bridge) module. In the figure, the associated 3D model of the anterior orbit boundary (AOB) is shown in blue. Surface reconstructed model is converted to label volume in 3D Slicer using "model to label sampling" and cutting with the AOB model using "label masking".

D. *Validation*

A dried skull of an Asian male adult is used to validate the proposed method. We adopted the traditional technique on orbit shape measurement. As shown in Fig. 1, we firstly block fissures and holes with wax. Then we applied impression (Vinyl Polysiloxane, Elite double 22, Zhermack SpA, Itlay) on the orbital walls of the dried skull. CT scan is taken on the dried skull along with the impression. Hounsfield window 200-350Hu is used to segment the impression. Other missed spaces in the orbit and air bubbles are filled slice by slice manually. Finally, the orbit models are cut with the AOB model.

III. RESULTS

Comparison of the segmentation results by using the proposed screened vertex surface reconstruction (SVR) and silicon impression is shown in Fig. 5. Axial slice views of the proposed vs orbital bone are shown in the upper row. Lower row shows the slices of the proposed vs impression. Fig. 6 shows 3D views of the superimposed models of the proposed vs impression (magenta). It can be seen that the results are very close. In TABLE I. , the volume, volume differences and root mean squared errors of the surface distance are also compared.

TABLE I. DIMENSIONAL COMPARISON OF THE ORBIT MODEL FROM IMPRESSION AND PROPOSED METHODS.

	Left orbit	**Right orbit**
Volume (impression, mm^3)	25074.96	25036.86
Volume (proposed method, mm^3)	25606.22	24656.68
Volume difference (%)	2.12	-1.52
Surface distance (RMS,mm)	0.458	0.369

IV. Conclusions

Traditional method using dental impression to the effective volume measurement of orbit requires much labor. It is time consuming but it is the gold standard. Existing segmentation methods save much material cost but still require manual adjustment. It is not favorable because of the operator variability's. In this paper, we suggested a computational approach to the orbit segmentation. Orbital bone model are firstly segmented using multiple Hounsfield unit thresholding method. 3D Orbit model is generated from Poisson reconstruction with automatically screened vertices from the inner orbit surfaces. Validation results show less than 2.2% volume difference to that obtained from impression method. Existing approaches with automation interpolate the label voxels by using some of the available slices or with some fixed points. In the proposed approach, it makes use of most of the data points from the orbital walls for the surface reconstruction as much as possible. Further works about the parameter model design, more validations and more detailed repeatability study are under investigation.

Acknowledgment

We would like to give our special thanks to Mr. Leung Mun Fai (Dental Laboratory Unit, Prince Philip Dental hospital).

References

[1] A. Weaver, K. Loftis, J. Tan, S. Duma and J. Stitzel, "CT Based Three-Dimensional Measurement of Orbit and Eye Anthropometry," Invest. Ophthalmol. Vis. Sci. 51(10), pp. 4892-4897, 2010.

[2] R. Bentley, S. Sgouros, K. Natarajan, M. Dover and A. Hockley, "Normal changes in orbital volume during childhood," J. Neurosurg. 96(4), pp. 742-746, 2002.

[3] J. Liu, S. Huang, A. Aziz and W. Nowinski, "Three dimensional digital atlas of the orbit constructed from multi-modal radiological images," Int. J. Comp. Assist. Rad. Surg. 1(5), pp. 275-283, 2007.

[4] C. Bender, W. Veneman, J. Veenland, I. Mathijssen, W. Hop, M. Koudstaal, E. Wolvius, "Orbital aspects following monobloc advancement in syndromic craniosynostosis," J. Cranio-Maxillofac Surg. 41(7), pp. e146-e153, 2013.

[5] L. Kamer, H. Noser, A. Schramm, B. Hammer, "Orbital form analysis: problems with design and positioning of precontoured orbital implants: A serial study using post-processed clinical CT data in unaffected orbits," Int. J. Oral Maxillofac. Surg. 39(7), pp. 666-672, 2010.

[6] A. Falcao. and J. Udupa, "A 3D generalization of user-steered live-wire segmentation," Med. Imag. Ana. 4(4), pp. 389-402, 2000.

[7] A. Schenk, G. Prause and H. Peitgen, "Efficient Semiautomatic Segmentation of 3D Ob-jects in Medical Images," MICCAI 1935, pp. 186-195, 2000.

[8] Y. Kang, K. Engelke and W. Kalender, "A new accurate and precise 3-D segmentation method for skeletal structures in volumetric CT data," IEEE Trans. Med. Imag. 22(5), pp. 586-598, 2003.

[9] J. Liu, H. Su and W. Nowinski, "A hybrid approach for segmentation of anatomic struc-tures in medical images," Int. J. Comp. Assist. Rad. Surg. 3(3-4), pp. 213-219, 2008.

[10] P. Scolozzi and B. Jaques, "Computer-aided Volume Measurement of Posttraumatic Orbits Reconstructed With AO Titanium Mesh Plates: Accuracy and Reliability," Ophthal. Plast. Recon. Surg. 24(5), pp. 383-389, 2008.

[11] N. Regensburg, P. Kok, F. Zonneveld, L. Baldeschi, P. Saeed, W. Wiersinga and M. Mourits, "A New and Validated CT-Based Method for the Calculation of Orbital Soft Tissue Volumes," Invest. Ophthalmol. Vis. Sci. 49(5), pp. 1758-1762, 2008.

[12] I. Nyström, J. Nysjö, and F. Malmberg, "Visualization and Haptics for Interactive Medical Image Analysis: Image Segmentation in Cranio-Maxillofacial Surgery Planning," Visual Informatics: Sustaining Research and Innovations, Lecture Notes in Computer Science. 7066, pp. 1-12, 2011.

[13] M. Kazhdan, M. Bolitho and H. Hopp, "Poisson surface reconstruction," Proc. 4th Euro-graph. sym. Geo. process., pp. 61-70, 2006.

[14] P. Yushkevich, J. Piven, H. Hazlett, R. Smith, S. Ho, J. Gee, G. Gerig, "User-guided 3D active contour segmentation of anatomical structures: Significantly improved efficiency and reliability," NeuroImage 31(3), pp. 1116-1128, 2006.

[15] A. Fedorov, R. Beichel, J. Kalpathy-Cramer, J. Finet, J. Fillion-Robin, S. Pujol, C. Bauer, D. Jennings, F. Fennessy, M. Sonka, J. Buatti, S. Aylward, J. Miller, S. Pieper, R. Ki-kinis, "3D Slicer as an Image Computing Platform for the Quantitative Imaging Network," Magn. Reson. Imag. 30(9), pp, 1323-41, 2012.

[16] MeshLab. Visual Computing Lab ISTI-CNR. Available from: http://MeshLab.sourceforge.net

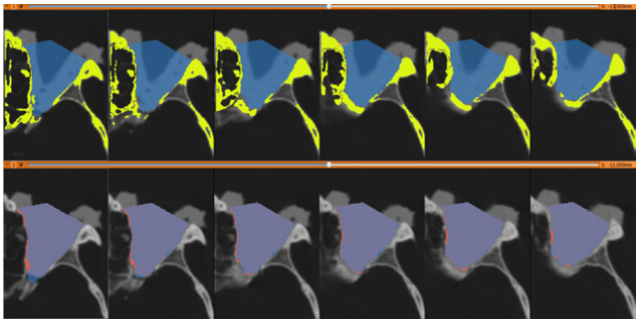

Fig. 5. Axial slice views of the segmentation result. Upper row: SVR (blue) vs orbital bone (yellow). Lower row are SVR vs impression (red).

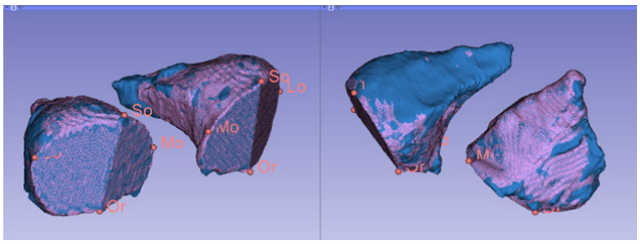

Fig. 6. Comparison of the segmentation results by using the proposed method (blue) and Hounsfield thresholding on the impression (magenta). Left: view from upper-right-anterior side. Right: view from lower-left-posterior side.